Acta Materialia 232 (2022) 117973

Contents lists available at ScienceDirect

Acta Materialia

journal homepage: www.elsevier.com/locate/actamat

Full length article

Molecular dynamics simulations of ultralow hysteretic behavior in super-elastic shape memory alloys

Xuefei Tao[a], Yang Yang[a], Hongxiang Zong[a,*], Xiangdong Ding[a,*], Kaiyuan Yu[b], Turab Lookman[c], Jun Sun[a]

[a] State Key Laboratory for Mechanical Behavior of Materials, Xi'an Jiaotong University, Xi'an, Shaanxi 710049, China
[b] Department of Materials Science and Engineering, China University of Petroleum-Beijing, Beijing 102246, China
[c] AiMaterials Research LLC, Santa Fe, New Mexico 87501, USA

ARTICLE INFO

Article history:
Received 15 March 2022
Revised 13 April 2022
Accepted 21 April 2022

Keywords:
Shape memory alloy
Superelasticity
Hysteresis
Martensitic transformation

ABSTRACT

Shape memory alloys (SMAs) that exhibit superelasticity with large recoverable strain and small hysteresis are in demand for practical applications, although their synthesis remains a challenge. We introduce metastable engineering to dope conventional SMA solid-solution atoms of relatively high concentration with "weak" local lattice distortion to realize ultralow hysteretic superelasticity. Large-scale molecular dynamic (MD) simulations of NiTi-based SMAs are performed to demonstrate how the presence of 2 ~ 4 at.% Nb dopants lead to a stress-induced transition from a metastable pretransitional state to a strain-glass state. This is facilitated by a macroscopically homogeneous and continuous phase transformation in the course of superelastic loading and unloading. This spinodal decomposition-like phase transformation process endows SMAs with anhysteretic superelasticity that is insensitive to loading direction and grain size (below 15 nm). These findings show promise of achieving ultralow hysteretic superelasticity with large recoverable strain for SMAs.

1. Introduction

Shape memory alloys (SMAs) undergo a reversible, diffusionless, structural phase transformation between parent and martensitic phases in response to external stimuli (temperature, stress, electric field, magnetic field, or combinations thereof), accompanied by strains ranging up to and beyond 10%. The ability to recover their initial shape after releasing the applied load, known as superelasticity (SE), makes them promising materials for energy absorption and ensuring the stability of structures under relatively large strains [1–5]. However, special attention needs to be paid to the phenomena of complex hysteresis associated with irreversibility, which ensures a reduction in the device performance [6–9] under loading due to the application of strain/stress control. Therefore, decreasing stress hysteresis in SMAs becomes a key issue to improve their performance. Low hysteresis is attractive as the temperature oscillation for the actuation force and/or displacement can then be small to facilitate a fast response.

Reducing the length scale of SMAs down to the nanoscale is one strategy that can decrease significantly the martensitic transformation (MT) hysteresis loop. Thus, research in nanoscale shape memory materials has focused on small-scale structures such as nano/micro pillars, wires and particles [10–14]. The hysteresis even disappears when the SMA particle size is decreased below 3 nm. In other words, anhysteretic superelasticity is achieved in SMA particles smaller than 3 nm [15]. At the other end of the scale lies bulk nanocrystalline SMAs with grain sizes in the range 5–150 nm synthesized by severe plastic deformation into an amorphous phase followed by recrystallization using heat treatments [16]. For both cases, the inhibition of MT within grain boundaries or free surface regions plays an important role in lowering superelastic hysteresis, i.e., a large volume fraction of SMAs is retained in the parent phase during the superelastic loading process, leading to vanishing hysteresis [15,16].

Yet another strategy towards the search for SMAs with small superelastic hysteresis is to use “domain engineering” to transform a sharp first-order MT into a continuous glasslike phase transition via impurity doping [17]. The presence of an appropriate density of extra defects (such as point defects, dislocations and nanoprecipitates) in coarse-grained SMAs can induce considerable local lattice distortion. This can prevent the sudden formation of long-range ordered martensitic twinned structures and can lead to the formation of randomly distributed, frustrated, nanoscale martensitic domains [18–20]. Such a unique strain state is found to evolve grad-

* Corresponding authors.
E-mail addresses: zonghust@mail.xjtu.edu.cn (H. Zong), dingxd@mail.xjtu.edu.cn (X. Ding).

https://doi.org/10.1016/j.actamat.2022.117973
1359-6454/

ually upon loading and unloading with narrow superelastic hysteresis due to the lack of MT nucleation and twinning/detwinning events. However, experimental measurements on the nano-domain engineered SMAs show that the reduction of superelastic hysteresis using this strategy is often accompanied by quasi-linear superelasticity with small recoverable strain [17,20,21]. Once the strain is very high, the large lattice mismatch between the parent phase and developed martensite gives rise to a high strain energy barrier for coarsening martensite, thus leading to a larger hysteretic loop [22,23].

Recently, anhysteretic superelastic behavior with large recoverable strain has been observed in a NiCoFeGa single-crystal alloy, a ferromagnetic SMA system. Kosogor et al. observed anhysteretic superelasticity in a Ni-Fe(Co)-Ga single-crystal alloy if the temperature exceeds a critical value of 320 K [24]. Later, Wang et al. reported "ideal" anhysteretic superelasticity in [001]-oriented NiCoFeGa single crystals, exhibiting a large recoverable strain up to 15.2%. *In-situ* synchrotron X-ray diffraction measurements suggest that the anhysteretic behavior is correlated with a stress-induced continuous variation of lattice parameter, as well as the atomic-level entanglement of ordered and disordered crystal structures upon loading and unloading [25]. Subsequent *ab initio* calculations indicate that a magnetic effect needs to be present to act as a dominating factor for the anhysteretic superelasticity response. For example, magnetic reversal (FM $\leftrightarrow$ AFM) may occur while stretching the B2 structure of $Ni_{50-x}Co_xMn_{25}Ga_{25}$ alloys [26]. However, this mechanism does not seem to work for well-studied SMAs such as NiTi without a magnetic effect or magnetic entropy. There is therefore a need to explore new mechanisms that can guide the development of bulk SMAs with narrow hysteretic superelasticity and large recoverable strain. Large-scale molecular dynamic (MD) simulations have emerged as an effective tool to study superelasticity in NiTi SMAs [27–30], providing an understanding of the corresponding atomic level phase transformation mechanisms.

In the present work, we demonstrate a mechanism to reduce superelastic hysteresis in conventional NiTi-based SMAs by engineering metastability, i.e. using "weak" local lattice distortions to realize a metastable pretransitional state. The metastable state induces a spinodal decomposition-like phase transformation, which has the potential of achieving an "ideal" superelasticity of narrow hysteresis and large recoverable strain. We perform MD simulations of NiTi-based SMAs, which are solid-soluted by alloying atoms with moderate local lattice distortion. We uncover spinodal decomposition-like phase transformation mechanisms for "ideal" superelastic behavior from the analysis of the corresponding atom-level microstructural evolution. In particular, the stress-induced continuous phase transition starting from the metastable pretransitional state is revealed. Finally, we discuss the potential doping elements that facilitate the presence of "ideal" low-hysteretic superelasticity.

2. Methodology

We performed MD simulations on a NiTi-based alloy to investigate superelastic behavior. The B2-NiTi structure has space group $Pm\bar{3}m$ with 2 atoms in the primitive unit cell and lattice parameters $a = b = c = 2.99$ Å, close to the 3.015 Å (an error less than 0.5%) value from experiments. By repeating the unit cell along *x*-, *y*- and *z*-axes, a supercell of pure NiTi can then be generated. Typical samples of NiTi-*X* alloys can be created by randomly replacing a given atomic concentration of Ti sites with dopant *X* atoms, i.e., the location of *X* atoms is arbitrary.

We consider $Ni_{50}Ti_{50-x}Nb_x$ ($x < 5$) alloys as an example in our simulations as Nb atoms can generate "weak" lattice distortions within NiTi-based SMAs. We focus on the effects of doping on the martensitic transformation behavior of an SMA random solid solution, in contrast to studying the composite structure formed experimentally in a eutectic reaction of NiTi-Nb alloys. From experimental work, $Ni_{50}Ti_{50-x}Nb_x$ ($x < 4$) shows a uniform B2 phase but with a different Nb content locally [31]. In addition, we also test the phase component of a 4% Nb sample ($Ni_{51.5}Ti_{44.5}Nb_4$) experimentally. Both scanning electron microscope (SEM) and synchrotron X-ray diffraction measurements indicate a B2 single phase, as shown in Fig. 1. In addition, a relatively recent study has suggested that the solubility of Nb can increase with an increasing Ni/Ti ratio [32]. Therefore, the alloy system $Ni_{50}Ti_{50-x}Nb_x$ (x<5) studied here can be experimentally accessible and we will demonstrate that the spatial variation of Nb concentration does not affect the narrow-hysteretic superelasticity.

We adapted a second nearest neighbor modified embedded-atom method (2NN MEAM) [33] to describe the Ni-Ti-*X* ternary system. An interatomic potential proposed by Ko et. al. [34] was used to describe the temperature and stress-induced phase transformation in NiTi. The parameters for the interaction between solid-solute atoms *X* and Ni/Ti were fitted based on faithfully reproducing the DFT calculation for the B2 *X*-Ni (or *X*-Ti) structure. We note that such a semi-empirical potential description is not expected to capture the details of the specific alloy, however, such approaches have been widely adopted for martensitic transformations and related phenomena [35,36].

The initial samples were relaxed by quenching with the aid of a conjugate gradient algorithm. The samples were then annealed above the parent phase stabilizing temperature by using a Nose-Hoover thermostat [37] and Parrinello–Rahman barostat [38] within the isothermal-isobaric ensemble. Tension was then applied to the relaxed samples at a strain rate of 4×10^{-4} ps^{-1}. A bond order parameter introduced by Ackland and Jones [39] is used to identify the local structures. The atomic simulations were carried out using the LAMMPS code [40] and the atomic configurations visualized by Ovito [41].

3. Results

3.1. Superelasticity and shape memory effect

We first performed MD simulations of the tensile superelastic behavior in $Ni_{50}Ti_{50-x}Nb_x$ alloy single-crystals along the [112] direction. Here, Nb atoms are randomly added to form a solid-solution of the B2-NiTi based alloy. Fig. 2 shows a series of stress-strain curves for single-crystal $Ni_{50}Ti_{50-x}Nb_x$ ($x = 0 \sim 4$) SMAs at 15 K, 100 K, 200 K and 400 K. The first difference is that the Nb concentration makes the recoverability of the stress-strain curves. At temperatures below 400 K, the pure NiTi alloy exhibits a shape memory effect, i.e., shape recovery can only be obtained by heating, while the strain recovery after unloading increases with the fraction of Nb atoms. Complete recovery is obtained with doping of 2 at% Nb or higher. This shows a change in transformation behavior from the shape memory effect to superelasticity due to the reduction of phase transformation temperature. Another striking change is the shape variation in the hysteresis curves. For the case of $x = 0$ at 400 K, the loading curve after the yield point shows a stress plateau related to the stable growth of martensitic transformation, and a flag-shaped sharp curve with a relatively large hysteresis is formed. However, with increasing Nb fraction, we see a rounding of the hysteresis loops: the wide and sharp hysteretic behavior changes to a narrower hysteresis. In addition, we find the slope of the stress plateau gradually increases with Nb concentration, and the stress-strain curve for $x = 4$ almost disappears without any clear yield points. Most of these simulation results agree with previous experimental measurements and phase field modeling. Nevertheless, it is important to point out that we find a composition region of $x = 2 \sim 3$ at low temperatures (around 100 K and be-

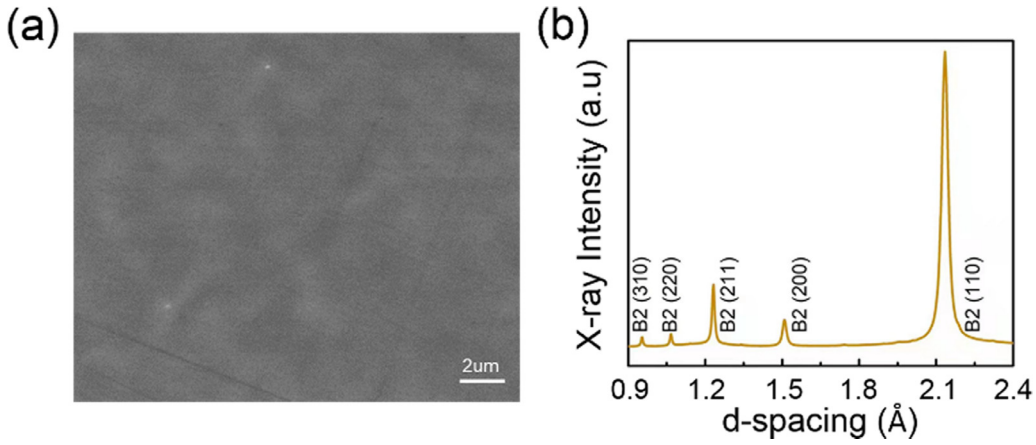

Fig. 1. Experimental measurement for $Ni_{51.5}Ti_{44.5}Nb_4$ alloy. (a) SEM morphology showing local compositional fluctuations. (b) Synchrotron X-ray diffraction measurement indicates a B2 single phase.

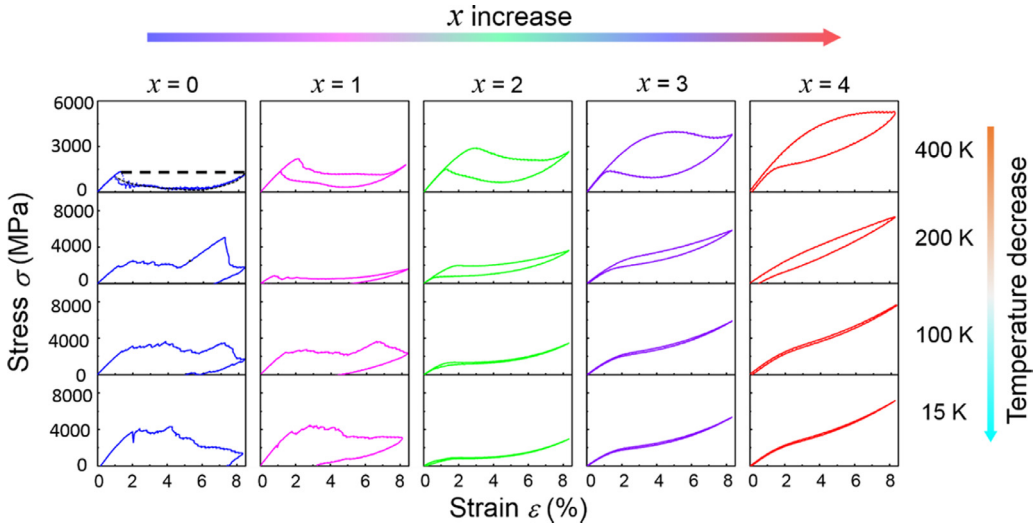

Fig. 2. Tensile stress-strain curves of $Ni_{50}Ti_{50-x}Nb_x$ ($x = 0 \sim 4$ at.%) alloy systems at selected temperatures. The superelastic hysteresis loop changes from a sharp and wide loop to a round, slim one with the amount of Nb atoms.

low) that surprising showing narrow-hysteretic superelasticity with a stress plateau. This shape of the stress-strain curve is very similar to "ideal" superelasticity found in NiCoFeGa single-crystal ferromagnetic SMAs [25,26]. In addition, we studied the case of 3Nb SMA with local Nb compositional fluctuation to mimic the experimental measurement, and the corresponding tensile stress-strain curve suggests a similar low-hysteretic superelasticity (see Fig. S1).

Next, we investigated the shape memory effect in $Ni_{50}Ti_{50-x}Nb_x$ alloys, i.e., martensitic transformation (MT) induced strain-output (ε) during load-biased thermal cycling. Fig. 3 shows the disorder dependence of the ε-T curve for $Ni_{50}Ti_{50-x}Nb_x$ SMAs during load-biased thermal cycling under different constant stresses. Solid and broken lines indicate heating and cooling runs, respectively. The 0 Nb pure alloy exhibits typical ε-T curves for NiTi shape memory alloys with large hysteresis. The transformation strain increases with increasing constant stress due to the growth of preferential martensitic domains. With increasing Nb dopants, the relatively sharp and wide hysteresis loop for 0 Nb alloy becomes rounded and narrow. In addition, there appears to be a threshold stress below which the transformation strain cannot be detected over the temperature region from 400 K to 15 K. In the 2 Nb alloy, for example, this behavior is clearly observed with a threshold stress of 500 MPa, in agreement with the corresponding superelastic behavior in Fig. 2, which shows the stress induced martensitic transformation over the whole temperature region of our simulations. The normal MT is completely suppressed if the doping level is further increased (e.g. the cases of 3 and 4 Nb alloys), even at high applied stress. More strikingly, the continuous increase in macroscopic strain for 3 and 4 Nb upon cooling at high applied stresses suggests a continuous MT process. It is quite different from strain-glass alloys (STG) [42–44]. In the case of STG, the strain-glass transition occurs without macroscopic symmetry breaking with applied low stresses, whereas a normal MT occurs if the applied stress is higher than a critical value.

3.2. Anisotropy

We have so far studied the mechanical response of single-crystal $Ni_{50}Ti_{50-x}Nb_x$ SMAs based on uniaxial tensile mode along the [112] direction. It is natural to ask if slim-hysteretic superelasticity exists in other loading directions. Fig. 4 compares the tensile superelastic behavior of 3 Nb samples along three high symmetry directions [111], [110] and [112]. We do not include the cases in which we load along the [001] direction, which can induce a large elastic strain that couples with the tetragonality (c/a >1.0) of the phase transformation [45]. Here, two different temperatures 100 and 400 K are selected to study the dependence of temperature on superelastic hysteresis. All the cases in Fig. 4 show complete recov-

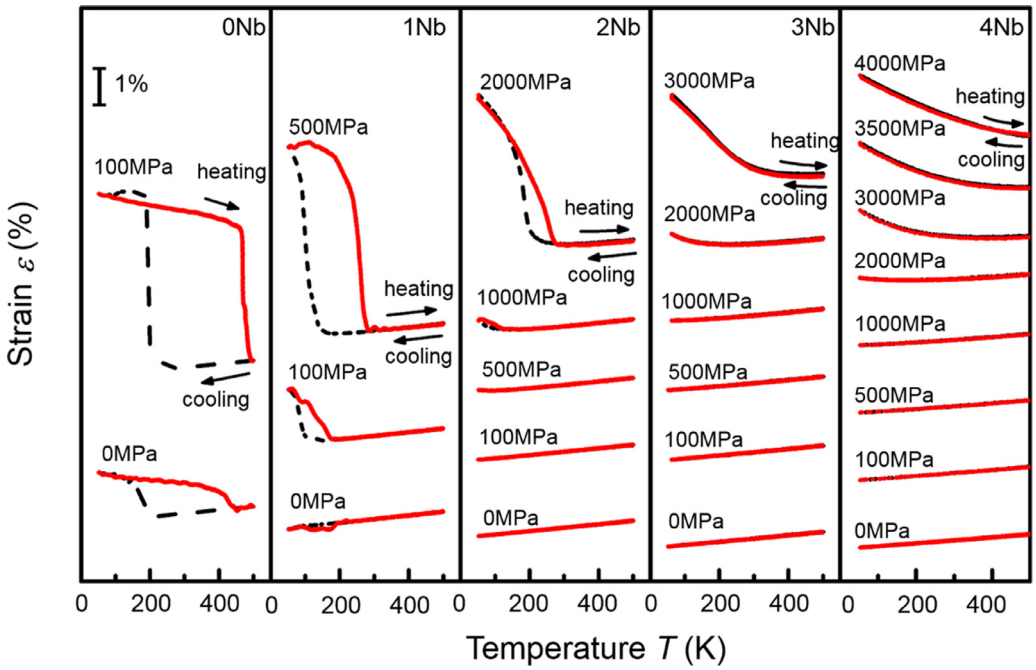

Fig. 3. Strain-temperature curves of $Ni_{50}Ti_{50-x}Nb_x$ ($x = 0 \sim 4$ at.%) shape memory alloys measured with the uniaxial tensile mode during load-biased thermal cycling under different stresses. The thermal hysteresis loop decreases with the concentration of Nb atoms, but the critical stress that can induce martensitic transformation increases with the Nb concentration.

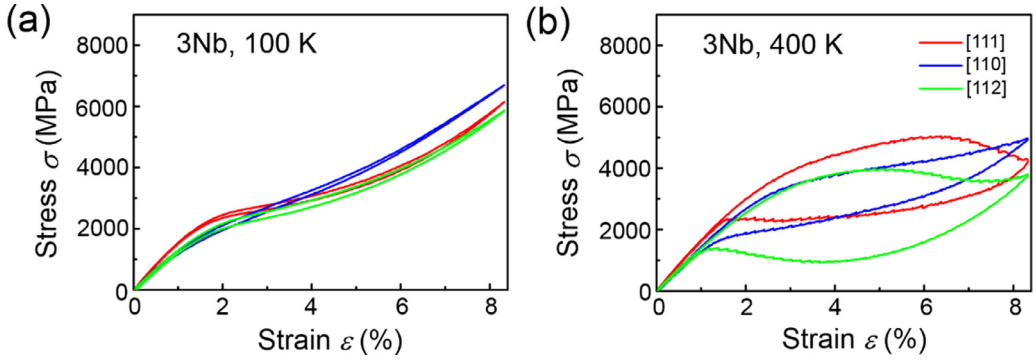

Fig. 4. The tensile loading direction dependent mechanical response of 3 Nb SMA samples. (a) Stress-strain curves at 100 K. (b) Stress-strain curves at 400 K. At low temperatures, the superelasticity of 3 Nb SMA shows low anisotropy.

erability in the tensile stress-strain curves. However, the anisotropy of the corresponding hysteretic behavior is quite different at temperatures 100 and 400 K. As shown in Fig. 4(b), the superelasticity of 3 Nb SMAs shows relatively large hysteresis along all three directions at 400 K with the hysteretic loops a function of the loading direction. For example, [110] and [112] exhibit the smallest and largest superelastic hysteresis, respectively. In contrast, the superelastic response at the low temperature 100 K is quite similar in different directions, i.e., 3 Nb SMA shows narrow hysteresis and comparable yield stress (Fig. 4(a)) with uniaxial tensile loading along the three directions. This suggests that the superelastic hysteresis of 3 Nb SMAs is insensitive to loading direction at low temperatures. The loading direction can change the stress plateau of the superelastic curves.

3.3. Size effect

Previous studies have indicated that the size of grains and other substructures (such as deformation twins) can significantly influence the stress-induced martensitic transformation in NiTi SMAs [46–49]. In particular, the superelastic hysteresis as well as the dependence of the plateau stress on temperature, decrease rapidly as the grain size is reduced beyond a critical value (< 60 nm) [50]. We thus investigated the superelastic behavior of $Ni_{50}Ti_{47}Nb_3$ SMAs in different grain sizes. Fig. 5(a) and (b) present the grain sizes dependent superelasticity at low (100 K) and high temperature (400 K), respectively. We can clearly observe a size effect on the superelastic stress by comparing the stress-strain curves for different grain sizes, i.e., the superelastic plateau stress increases as the nano-grain sizes decrease from 15 nm to 3 nm, which is consistent with the usual grain boundary strengthening or Hall-Petch behavior. However, the dependence of the superelastic hysteresis on grain sizes is quite different. At 400 K, the superelastic hysteresis is reduced sharply as the grain sizes decrease (Fig. 5(b)). In sharp contrast, the 3 Nb alloys at 100 K show a weak size dependence, i.e., there is no significant change in the stress hysteretic loop when the grain sizes are reduced, as shown in Fig. 5(a). In summary, we can state that the hysteretic behavior of the 3 Nb nanocrystalline alloy is not sensitive to grain size (< 15 nm).

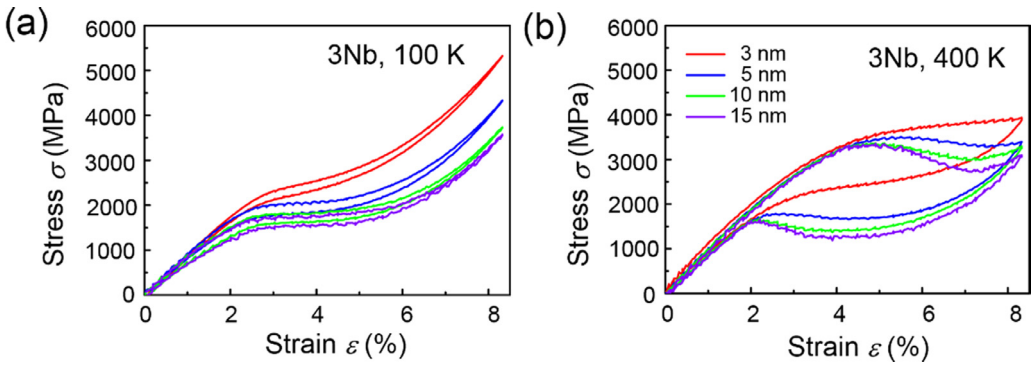

Fig. 5. Size effect on the mechanical response of different grain sizes SMA samples upon uniaxial tensile loading. We compared the tensile superelastic behaviors in 3 Nb samples with sizes of 15 nm, 10 nm, 5 nm and 3 nm at (a) 100 K and (b) 400 K, showing that the low-hysteretic behavior is independent of the grain sizes.

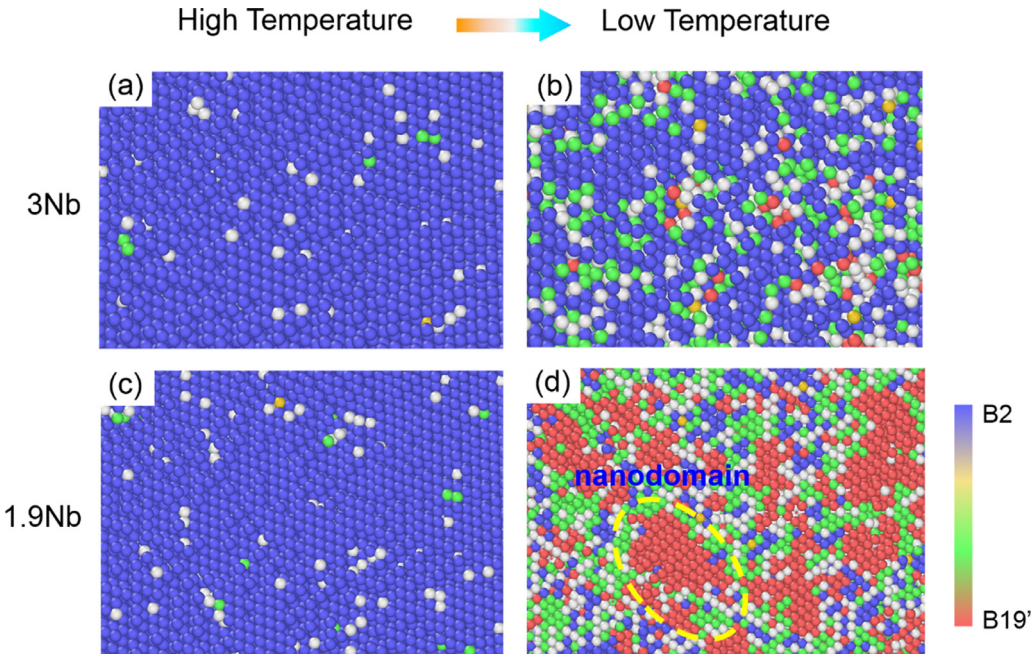

Fig. 6. Typical microstructural evolution of NiTi-based shape memory alloys upon cooling. (a) and (b) Local structure in 3 Nb alloy when the temperature is reduced from 400 K to 100 K. (c) and (d) Microstructural evolution in 1.9 Nb alloy upon cooling. The yellow circle shows a typical martensite nanodomain. The light blue color represents the ideal bcc structure, green is the distorted bcc structure, the orange represents the ideal monoclinic structure, and other colors belong to defects. (For interpretation of the references to colour in this figure legend, the reader is referred to the web version of this article.)

4. Discussion

MD simulations of the tensile superelastic behavior in $Ni_{50}Ti_{50-x}Nb_x$ SMAs show narrow hysteresis at low temperatures (around 100 K and below) as we dope Nb atoms in the composition range $x = 2 \sim 3$ at%. However, we do not detect any transformation strain upon cooling in the ε-T curves of Fig. 3, quite different from previous studies on nanodomain engineered SMAs [51]. The question naturally arises whether there is a difference in the underlying mechanisms for ultralow hysteretic superelastic behavior presented here and nanodomain engineered SMAs. We suggest that the "ideal" superelasticity in $Ni_{50}Ti_{50-x}Nb_x$ SMAs is dominated by a stress-induced continuous phase transformation. In the following, we will first investigate the difference between the 3 Nb SMA and nanodomain engineered SMAs [17] from the aspect of local structure and relaxation behaviors. We then analyze the microstructure evolution in the superelastic loading and unloading processes to gain insight into the underlying mechanisms. Finally, we propose a general criterion for achieving "ideal" superelasticity of narrow hysteresis and large recoverable strain, motivating experimental studies.

4.1. Local structure and relaxation behavior upon cooling

We have so far shown that the heavily Nb doped NiTi shape memory alloys exhibit superelasticity of large recoverable strain, low hysteresis and low working temperature range. Several theoretical models attribute the narrow hysteretic superelasticity in NiTi-*X* (*X* is dopant element) SMAs to the induced martensitic nanodomains by quenched disorder [17,52,53]. Therefore, we first examined the atom-level microstructures in $Ni_{50}Ti_{50-x}Nb_x$ alloys before tensile loading. Fig. 6 compares the typical microstructural change of the 3 Nb alloy upon cooling with that of the 1.9 Nb alloy that undergoes a freezing process with martensite nano-domains. The left panel shows the atom-level microstructure of both materials at high temperature, which shares similar features to the parent phase structure. However, the corresponding microstructure at low temperature is quite different. As shown in Fig. 6(b), no obvious

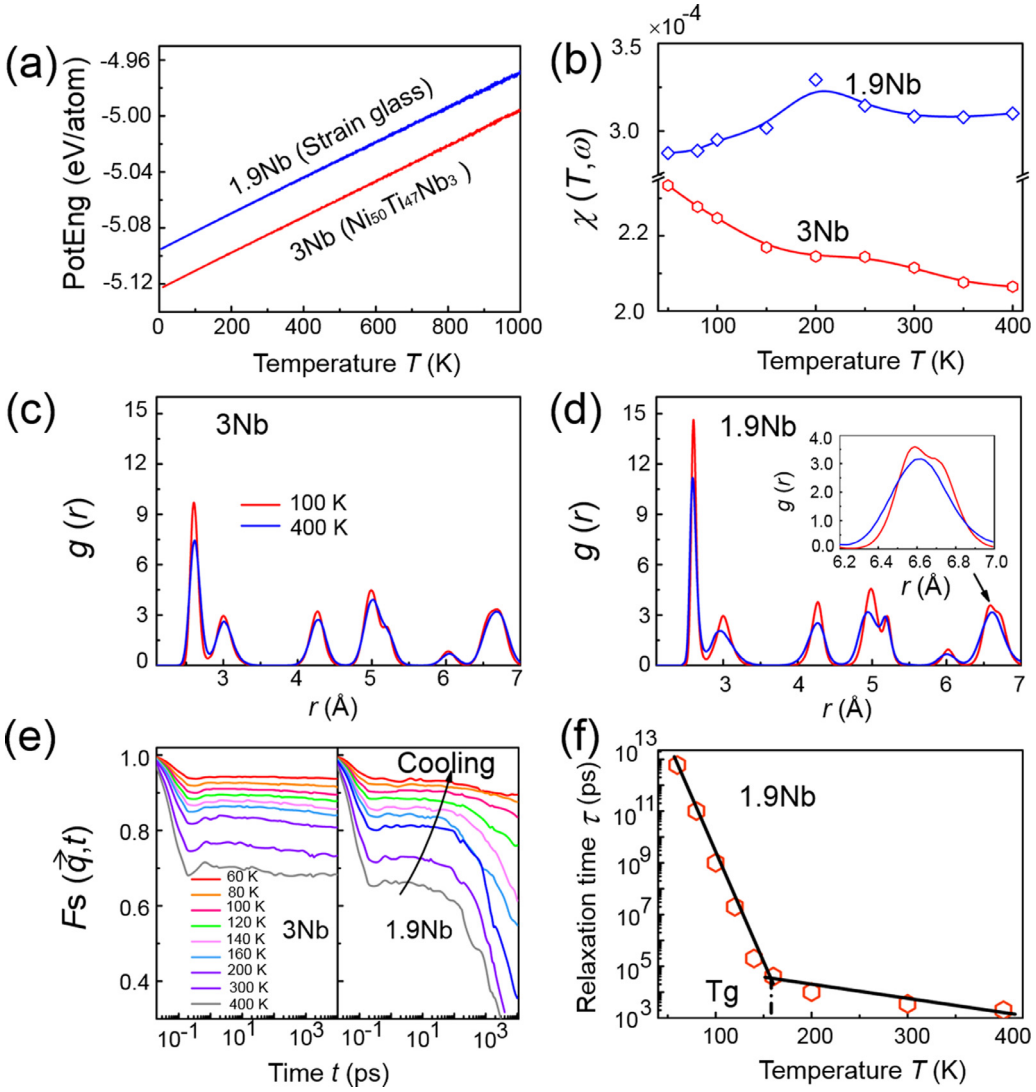

Fig. 7. Comparison of the dynamic behaviors between strain-glass alloys and metastable engineered shape memory alloys. (a) The dependence of potential energy on temperature. (b) Dynamic susceptibility as a function of temperature. (c) and (d) Radial distribution functions (RDFs) of 1.9 Nb SMA and 3 Nb SMA, respectively. (e) Intermediate scattering functions as a function of the time $F_S(\vec{q}, t)$ for the two different materials at different temperatures. (f) Plot of the relaxation time τ as a function of temperature, and τ is achieved via fitting the decay regimes of $F_S(\vec{q}, t)$ to the Kohlrausch-William-Watts (KWW) function. The characteristic feature of these physical properties suggests that metastable engineered 3 Nb SMA is in essence not in the strain-glass state.

martensite nanodomains (orange clusters) appear in the 3 Nb SMA sample. Instead, we find a high density of local metastable regions (green clusters) with distorted bcc structures. The microstructure is quite different from that of the strain-glass state (Fig. 6(d)), i.e., frozen martensitic nanodomains that are embedded within a distorted parent phase matrix or system-spanning strain network [18].

We next investigate the dynamic behavior of the alloys as a function of temperature, as shown in Fig. 7. Upon cooling, the change of potential energy for both 3 Nb and 1.9 Nb alloys is continuous, indicating no signature of a first-order martensitic transformation in both cases (Fig. 7(a)). This is confirmed by the corresponding radial distribution functions (RDFs), which can be used to characterize the structural information at a particular temperature. Fig. 7(c) and (d) compare the RDFs of both cases, and no significant change in their first three peaks suggests the average parent phase structure remains unchanged when the temperature is reduced from 400 K to 100 K. Note that there is no peak splitting in the RDF of the 3 Nb sample at low temperatures, as compared to the 1.9 Nb strain-glass alloy. Previous work on strain glasses has indicated that the peak splitting at long pair distance within the RDFs is due to the formation of strain networks due to local displacement shifts [18].

Fig. 7(b) shows the dynamic susceptibility of both 3 Nb and 1.9 Nb alloys at different temperatures. Here, the dynamic susceptibility is defined by $\chi(T, \omega) = \Delta(T, \omega)/T$, where $\Delta(T, \omega)$ measures the mean-squared displacement (MSD) of the system after a time interval of $1/\omega$, and plays a role analogous to the ac magnetic or dielectric susceptibility at frequency ω in experiments. As presented in Fig. 7(b), the evolution of $\chi(T, \omega)$ during the cooling process differs considerably between the two types of SMAs. On the one hand, compared with the 3 Nb case, the 1.9 Nb alloy possesses a higher value of $\chi(T, \omega)$ over the whole temperature region. On the other, the resulting curve of temperature dependence in 1.9 Nb alloy shows a cusp-like anomaly at around 150–200 K, indicating the presence of glassy behavior. Nevertheless, the observed susceptibility of 3 Nb SMA keeps increasing as the temperature is reduced.

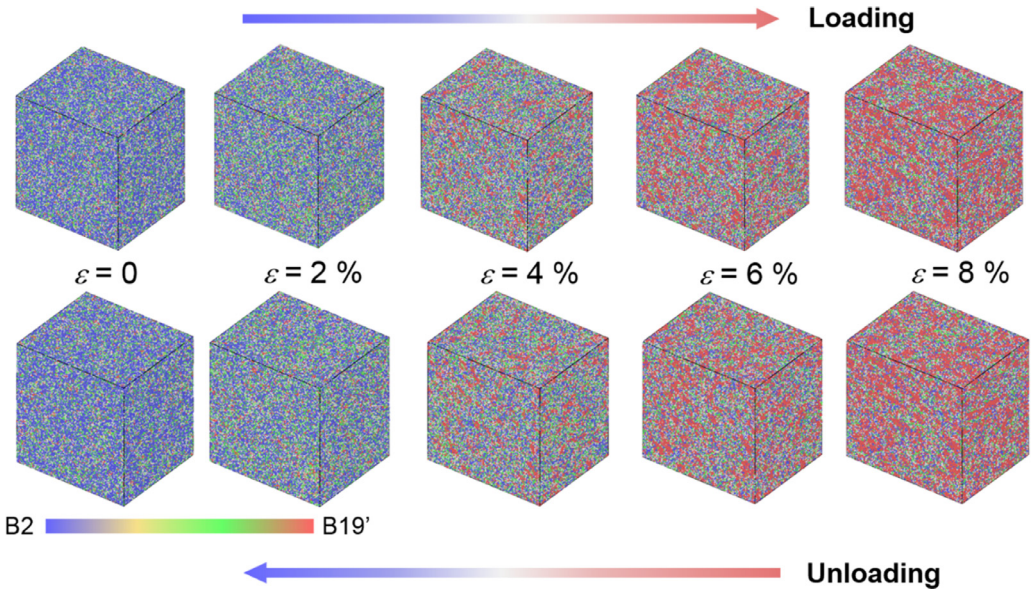

Fig. 8. Microstructure evolution of 3 Nb shape memory alloy during tensile loading and unloading at 100 K. Spinodal-decomposition–type pattern evolution kinetics dominates the stress-induced formation of new phase during the loading cycle. The light blue color represents the ideal bcc structure, green is the distorted bcc structure, the orange represents the idealmonoclinic structure, and other colors belong to defects. (For interpretation of the references to colour in this figure legend, the reader is referred to the web version of this article.)

We investigated the possible relaxation behavior in 3 Nb SMAs with the intermediate scattering function (ISF) [54], given by

$$F_S(\vec{q},t) = \frac{1}{N}\sum_{i=1}^{N} e^{i\vec{q}\cdot\left[\vec{r_i}(t)-\vec{r_i}(0)\right]} \quad (1)$$

where N denotes the atomic number and r_i is the position of atom i. The wave vector q is around 3.0 $Å^{-1}$, corresponding to the location of the first peak in the structure factor. The right panel of Fig. 7(e) shows the normal ISFs of 1.9 Nb SMA at different temperatures around the glass transition. The ISFs shows a fast drop, corresponding to the ballistic regime. The long-time decay in the following regime represents the α relaxation. Fig. 7(f) shows the temperature dependence of the fitted relaxation times, displaying two drastically different regions separated by the glass transition temperature T_g. In particular, we see orders of magnitude slowing down in the relaxation kinetics below T_g, which is typically observed experimentally in highly doped SMAs [51,55]. In contrast, the ISFs of 3 Nb SMA experience a first decay followed by a plateau that survives over the timescales of our simulations at all the selected temperatures, as shown in the left panel of Fig. 7(e). This suggests that large atomic re-arrangements or change of local structure is largely impeded except for thermally induced lattice vibrations. In short, all the features of the calculated observables above suggest that the 3 Nb alloy does not fall into the category of strain-glass or normal MT alloy.

4.2. Microstructural evolution and order parameters upon loading

We now consider the phase-transforming kinetics of 3 Nb SMAs accompanying the superelastic loading and unloading. Fig. 8 shows snapshots of atomic configurations during the tensile loading and unloading process at several strain levels. Surprisingly, the martensitic transformation in 3 Nb alloy starts uniformly throughout the sample and proceeds smoothly over the whole loading process, which is characteristic of the spinodal decomposition (SD) transformation in multicomponent alloys [56,57]. This is quite different from the case of a normal MT process, in which a new phase is nucleated and continues to grow under further loading (nucleation and growth, NG). As a result, the phase transformation process consists of large avalanches, exhibiting a sharp hysteresis loop [20]. However, we note that there is no difference between the lattice structure of martensite within $Ni_{50}Ti_{50}$ SMA and the 3 Nb alloy (Fig. S2).

The SD-like martensitic transformation process in the superelasticity of 3 Nb SMAs is confirmed by the distribution of the order parameter, as shown in Fig. 9. In the present work, the order parameter, η is defined as the lattice distortion associated with the B2 to B19' transformation [58]. Here, we introduce systematic coarse graining to pick up the correlated nature of local order parameters, i.e., the coarse graining of local η for each atom is calculated by averaging over all atoms within a length of 3.5 nm. In the course of a stress-induced martensitic transformation, the characteristic temporal change in probability distribution of the order parameter, $\varphi(\eta)$ exhibits a gradual, continuous change in the peak position for the 3 Nb case at 100 K (Fig. 9(a)), which is characteristic of SD-type phase ordering [56,57]. This is markedly different from the case of 0 Nb, which exhibits the bimodal distribution during tensile loading, characteristic of NG-type phase ordering [56,59] (see Fig. 9(b)). This suggests the presence of the sharp interface between parent phase and martensite is responsible for the large superelastic hysteresis in normal SMAs. In this way, both the superelasticity of 3 Nb at 400 K and 1.9 Nb at 100 K can be described as a mixed nature of SD-type and NG-type phase transformation, as shown in Fig. 9(c) and (d). For nano-domain engineered SMAs [17], a high proportion of the SD-type phase transformation during the loading-unloading process gives rise to narrow superelastic hysteresis. However, there still exists a considerable NG-type component, leading to quasi-linear superelasticity (Fig. 9(d)).

The Landau theory has been used to describe first-order martensitic transformations and shows the hysteretic behavior of shape memory alloys. Unlike a second-order phase transition, there is an energy barrier between the parent phase and martensite upon cooling when approaching the transformation temperature. The energy barrier gives rise to the highly hysteretic superelasticity. In most cases, the high strain energy barrier of nucleating martensite is due to a large lattice mismatch between the two phases, which is also the reason for the large recoverable strain. As illustrated in Fig. 10(b), the local stress induced by pre-existing

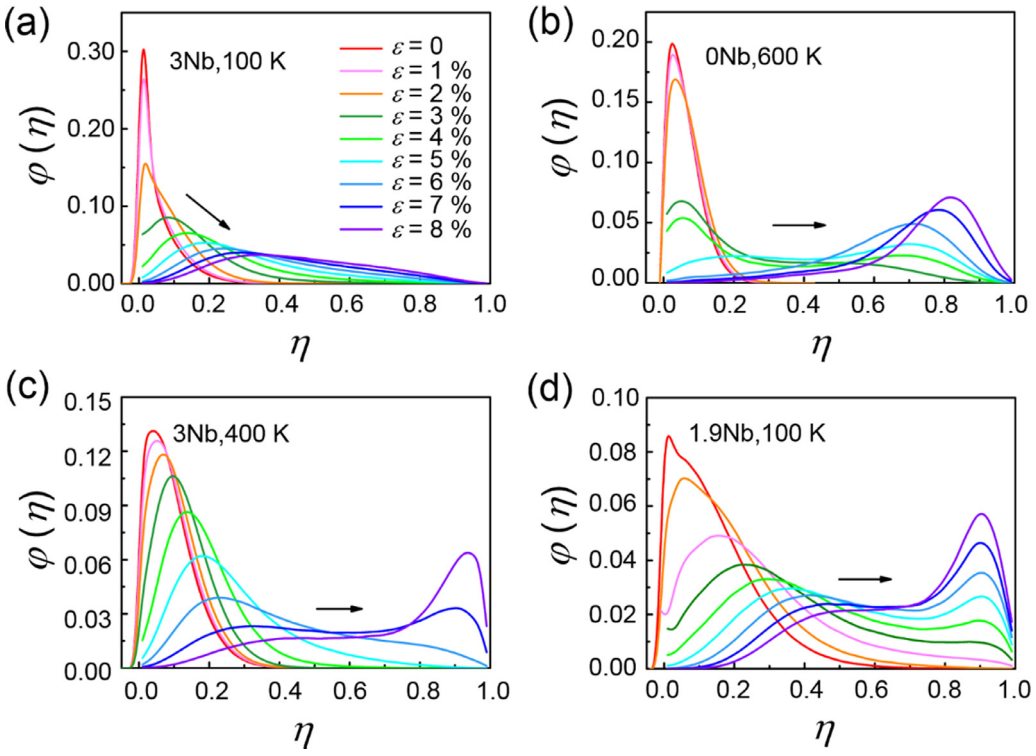

Fig. 9. Time evolution of the probability distribution of the order parameter for different NiTi-based shape memory alloysupon tensile loading. The probability distribution function of order parameter, $\varphi(\eta)$ at 9 different strain levels is presented for each case and the arrows represent the direction of the change with time. (a) Metastable engineered SMA of 3 Nb at 100 K. (b) $Ni_{50}Ti_{50}$ SMA at 600 K. (c) 3 Nb SMA at 400 K. (d)1.9 Nb SMA at 100 K.

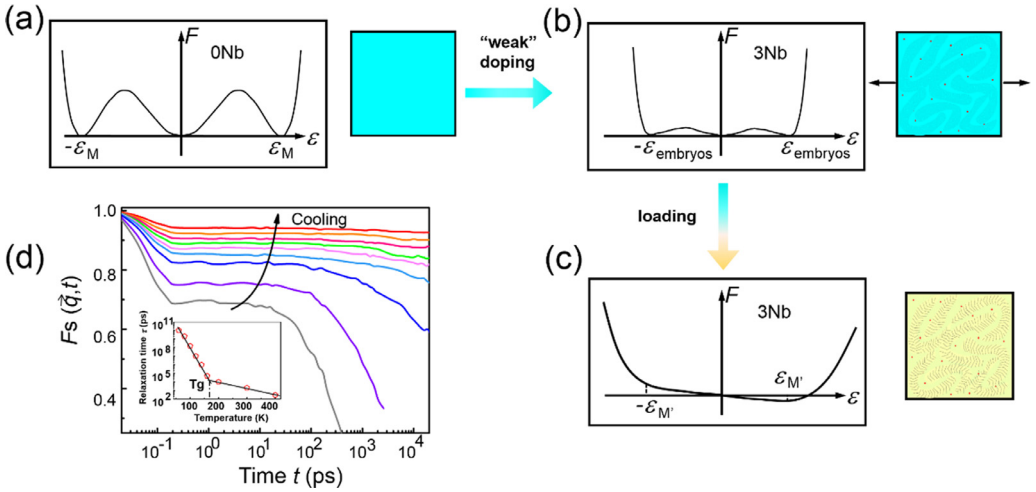

Fig. 10. Proposed phase transformation mechanism response for slim hysteretic superelasticity in metastable engineered shape memory alloys. Schematic illustration of stress-induced continuous phase transformation dominating the superelastic behavior at low temperatures. The schematic free-energy landscape of the (a) 0 Nb, (b) 3 Nb and (c) 3 Nb under loading. (d) Intermediate scattering functions as a function of the time, $F_S(\vec{q}, t)$ for 4.5% tensile-strain loaded 3 Nb sample, showing relaxation behaviors of glassy materials. The inset plots the fitted relaxation time as a function of temperature, indicating a glass transition at $T_g = 160$ K.

crystal defects in the pretransitional state of NiTi SMA can reduce or eliminate the nucleation barrier. This can trigger a nearly barrierless MT forming nanosized martensitic embryos due to thermoelastic equilibrium [60,61]. These embryos are always equilibrium coherent nanosized particles (Fig. 10(b)), physically different from the conventional fluctuation-assisted nuclei at low temperature, which are nonequilibrium particles that equilibrate by growing until they reach macroscopic dimensions.

For the cases of $Ni_{50}Ti_{50-x}Nb_x$ ($x = 2 \sim 4$), the local stress generated by Nb dopants is not strong enough to induce a localized MT, even by cooling to extremely low temperature. Therefore, no embryos could be observed in the absence of an applied field (Fig. 10(b)). We refer shape memory alloys of such latent instability as metastable engineered SMAs. However, on application of an external field, which provides an additional driving force, leads to the reversible and anhysteretic formation of embryos as shown in Fig. 10(c). Upon further loading, the sizes of nanosized embryos and their volume fraction grow smoothly as a function of external strain (Fig. 10(c)), and is responsible for narrow hysteretic superelasticity.

In addition, we investigated the structural relaxation dynamics of SMAs in the presence of stress-induced nanosized martensitic

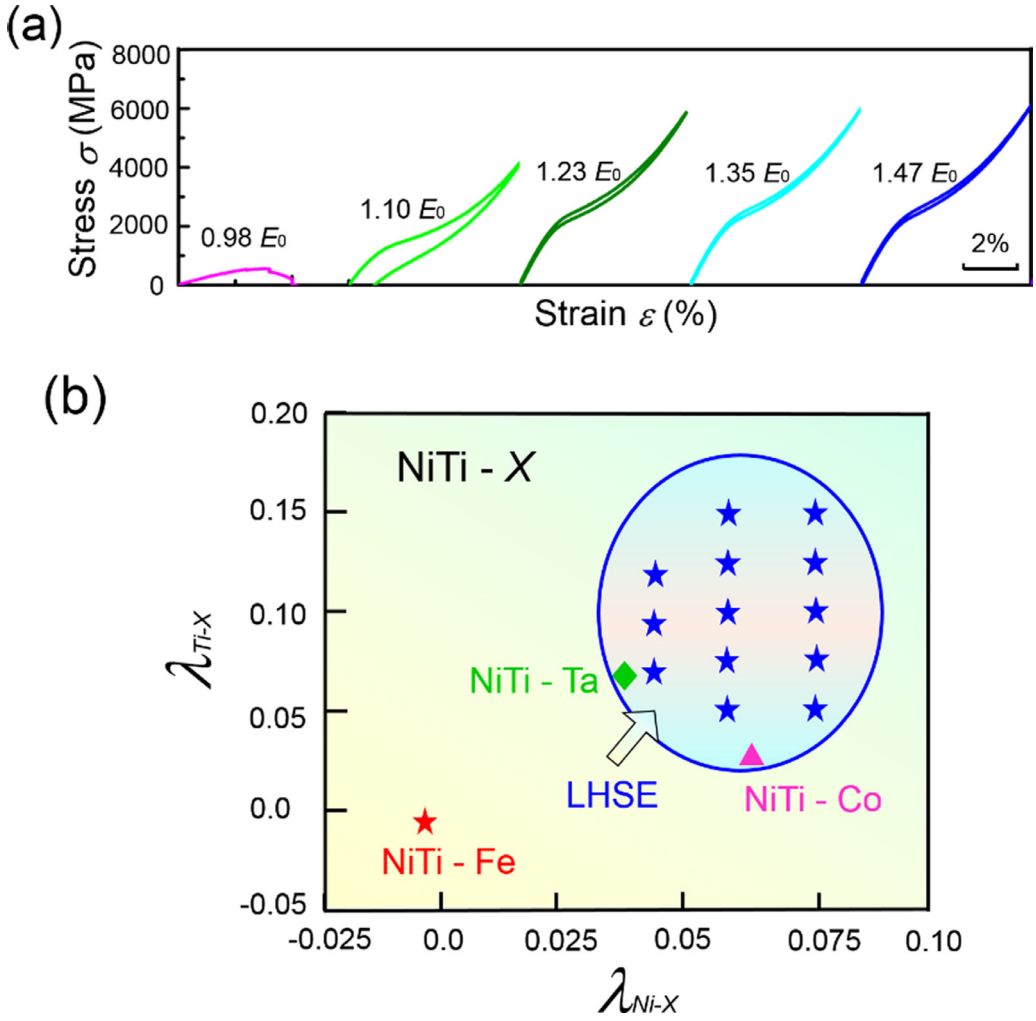

Fig. 11. Potential parameters for tuning superelastic hysteresis in NiTi-*X* shape memory alloys at 100 K. (a) Influence of the mixing enthalpy on the superelastic behavior in NiTi-*X* alloys. (b) Phase diagram of superelastic hysteresis spanned by the reduced interatomic distance of λ_{Ni-X} and λ_{Ti-X}, showing the effect of dopant atom size. E_0 represents the enthalpy of solution for *X* atoms within the Ni-Ti alloy. LHSE represents the low hysteretic superelastic effect.

embryos. Fig. 10(d) shows the ISF (Eq. (1)) of 4.5% tensile loaded 3 Nb sample at selected temperatures. Similar to glassy materials, the ISF curves possess long-time decay, indicating the presence of α relaxation. Accordingly, the fitted relaxation times display orders of magnitude slowing down in the relaxation kinetics (the inset of Fig. 10(d)), which is critical evidence for a glass transition [18,51]. As such, our work suggests that the anhysteretic superelasticity in 3 Nb SMAs at low temperatures originates from a stress-induced transition from pretransitional state to strain-glass state, which occurs continuously in a spinodal decomposition-type manner. We point out there should be no obvious difference between thermally-induced glassy behavior and the stress-induced glassy behavior shown in the present work. Both are mediated by a continuous formation of nano-martensite domains, instead of the sudden formation of long-range ordered domains. However, applied stress can be regarded as a new degree freedom to influence the change the landscape of "random field" [62] in 3 Nb SMA and the corresponding microstructural morphology, i.e., the number of nano-martensite domains increase continuously as a function of stress (see Fig. 8).

This picture agrees with recent experiments on Ti–Nb-based gum metals, which show similar superelastic behavior after introduction of concentration of dopant or interstitial oxygen atoms [20]. The signature of glassy behavior is even more acute after the process of cold rolling, indicating the presence of stress-induced continuous phase transformation, which starts from a metastable parent phase [63]. Also, previous studies of Fe-Pd based alloys [45] and single-crystalline Ni–Fe(Co)–Ga shape memory alloys [24] attribute the low-hysteretic superelasticity to a post-critical state, where the alloys undergo a continuous (second-order-like) phase transformation during tensile loading and unloading.

4.3. Role of dopant atomic size and enthalpy of mixing

Previous theoretical studies have pointed out that solute atoms can influence the martensitic transformation in two aspects. One is the chemical effect, which alters the relative stability of austenite and martensite via changing their enthalpy. The other is the local field effect, i.e., the creation of local stress prevent the transformation of the system into a single-phase state [62], because the thermally activated nucleations or nanosized martensite domains are pinned by the local stress field. Inspired by this, we investigated the potential screening physical parameters that can engineer metastability in NiTi-based SMAs. The influence of mixing enthalpy change on the superelastic behavior is presented in Fig. 11(a). For a specific doping concentration, a relatively high mixing enthalpy can help to reduce the global transformation temperature [18], thus facilitating the survival of a pretransitional

state in a low temperature range. Fig. 11(b) shows the phase diagram spanned by the reduced interatomic distances λ_{Ni-X} and λ_{Ti-X} (X is dopant element). Here, $\lambda_{Ni-X} = (r_{Ni-X} - r_{Ni-Ti})/r_{Ni-Ti}$ and $\lambda_{Ti-X} = (r_{Ti-X} - r_{Ni-Ti})/r_{Ni-Ti}$, and r is the nearest neighbor distance within their most stable B2 lattices. We find the anhysteretic superelasticity only appears in a narrow region of the phase diagram in Fig. 11(b) where both r_{Ni-X} and r_{Ti-X} are slightly larger than r_{Ni-Ti}. However, further increase of r_{Ni-X} and r_{Ti-X} can induce a stronger local stress field and the formation of local martensitic domains. This indicates that the local field induced by point defects should be “weak”, which can reduce the stability of a local pretransitional state but is not enough to overcome the kinetic barrier, in order to achieve the metastable engineered state in NiTi SMAs. More importantly, the "weak" local lattice distortion caused by doping Nb can produce a larger recoverable strain than that imposed by the effects of grain boundaries and amorphous phase since the latter case includes a high volume fraction of non-transforming region/phase [64–66].

Based on this criterion, we can screen potential NiTi-based alloys with similar low-hysteretic superelasticity. For example, both Ta and Co dopants are located within the low hysteretic superelastic effect (LHSE) region, whereas Fe dopants are not, as shown in Fig. 11(b). As expected, both of the alloys $Ni_{50}Ti_{47}Ta_3$ at 50 K and $Ni_{50}Ti_{45}Co_5$ at 20 K can show similar superelasticity with low hysteresis in the low temperature region (Fig. S3). However, NiTiFe alloys show the typical superelastic feature associated with nano-domain engineered SMAs [17].

5. Conclusions

We have shown a mechanism that can induce anhysteretic superelastic behavior by means of metastable engineering. Our molecular dynamic simulations showcase the novel mechanical performance in a model SMA system of $Ni_{50}Ti_{50-x}Nb_x$ ($x = 2 \sim 4$) when engineered with a high density of local metastability into the pretransitional phase. Our findings can be summarized as follows: (1) The metastable engineered SMAs show tensile superelasticity of narrow hysteresis, which is independent of loading directions and grain size; (2) The presence of dopant atoms with "weak" local lattice distortion and high enthalpy of solution above a critical concentration can suppress the frozen martensitic nano-domains as well as glassy relaxation behavior in SMAs; (3) The anomalous superelastic behavior is attributed to a stress-induced continuous phase transformation starting from the metastable pretransitional state, which occurs in a spinodal-decomposition-like fashion. Recently high-entropy or complex concentrated SMAs have emerged as a relatively new category of materials. These provide a wider space and stage to test the present findings experimentally.

Declaration of Competing Interest

The authors declare that they have no known competing financial interests or personal relationships that could have appeared to influence the work reported in this paper.

Acknowledgments

This work was supported by the National Natural Science Foundation of China (51931004, 51871177 and 52171011), the China Postdoctoral Science Foundation (2020M673385) and the 111 project 2.0 (BP2018008).

Supplementary materials

Supplementary material associated with this article can be found, in the online version, at doi:10.1016/j.actamat.2022.117973.

References

[1] K. Otsuka, C.M. Wayman, Shape Memory Materials, Cambridge University Press, 1999.
[2] K. Otsuka, X. Ren, Physical metallurgy of Ti–Ni-based shape memory alloys, Prog. Mater. Sci. 50 (2005) 511–678.
[3] L. Xue, K.C. Atli, S. Picak, C. Zhang, B. Zhang, A. Elwany, R. Arroyave, I. Karaman, Controlling martensitic transformation characteristics in defect-free NiTi shape memory alloys fabricated using laser powder bed fusion and a process optimization framework, Acta Mater. 215 (2021) 117017.
[4] Y. Tanaka, Y. Himuro, R. Kainuma, Y. Sutou, T. Omori, K. Ishida, Ferrous polycrystalline shape-memory alloy showing huge superelasticity, Science 327 (2010) 1488–1490.
[5] H. Huilong, S. Emrah, M. Tao, N.S. Johnson, Q. Suxin, C. Cheikh, S. Drew, A.H. Naila, Z. Lin, H. Yunho, Fatigue-resistant high-performance elastocaloric materials made by additive manufacturing, Science 366 (2019) 1116–1121.
[6] D. Zhao, J. Liu, X. Chen, W. Sun, Y. Li, M. Zhang, Y. Shao, H. Zhang, A. Yan, Giant caloric effect of low-hysteresis metamagnetic shape memory alloys with exceptional cyclic functionality, Acta Mater. 133 (2017) 217–223.
[7] L. Petrini, F. Migliavacca, Biomedical applications of shape memory alloys, J. Metall. 2011 (2011) 1–15.
[8] C. Chluba, W. Ge, R. Lima de Miranda, J. Strobel, L. Kienle, E. Quandt, M. Wuttig, Ultralow-fatigue shape memory alloy films, Science 348 (2015) 1004–1007.
[9] L. Mañosa, A. Planes, Materials with giant mechanocaloric effects: cooling by strength, Adv. Mater. 29 (2017) 1603607.
[10] D.C. Dunand, P. Müllner, Size effects on magnetic actuation in Ni-Mn-Ga shape-memory alloys, Adv. Mater. 23 (2021) 216–232.
[11] J.F. Gómez-Cortés, M.L. Nó, I. López-Ferreño, J. Hernández-Saz, S.I. Molina, A. Chuvilin, J.M. San Juan, Size effect and scaling power-law for superelasticity in shape-memory alloys at the nanoscale, Nat. Nanotechnol. 12 (2017) 790–796.
[12] W.F. Rao, M. Wuttig, A.G. Khachaturyan, Giant nonhysteretic responses of two-phase nanostructured alloys, Phys. Rev. Lett. 106 (2011) 105703.
[13] T. Waitz, K. Tsuchiya, T. Antretter, F.D. Fischer, Phase transformations of nanocrystalline martensitic materials, MRS Bull. 34 (2009) 814–821.
[14] Z. Du, X.M. Zeng, Q. Liu, C.A. Schuh, C.L. Gan, Superelasticity in micro-scale shape memory ceramic particles, Acta Mater. 123 (2017) 255–263.
[15] Z. Zhang, X. Ding, J. Sun, T. Suzuki, T. Lookman, K. Otsuka, X. Ren, Nonhysteretic superelasticity of shape memory alloys at the nanoscale, Phys. Rev. Lett. 111 (2013) 145701.
[16] M. Peterlechner, T. Waitz, H.P. Karnthaler, Nanocrystallization of NiTi shape memory alloys made amorphous by high-pressure torsion, Scr. Mater. 59 (2008) 566–569.
[17] D. Wang, S. Hou, Y. Wang, X. Ding, S. Ren, X. Ren, Y. Wang, Superelasticity of slim hysteresis over a wide temperature range by nanodomains of martensite, Acta Mater. 66 (2014) 349–359.
[18] H. Zong, H. Wu, X. Tao, D. Xue, J. Sun, S.J. Pennycook, T. Min, Z. Zhang, X. Ding, Percolated strain networks and universal scaling properties of strain glasses, Phys. Rev. Lett. 123 (2019) 015701.
[19] S. Sarkar, X. Ren, K. Otsuka, Evidence for strain glass in the ferroelastic–martensitic system $Ti_{(50-x)}Ni_{(50+x)}$, Phys. Rev. Lett. 95 (2005) 205702.
[20] Y. Nii, T.H. Arima, H.Y. Kim, S. Miyazaki, Effect of randomness on ferroelastic transitions: disorder-induced hysteresis loop rounding in Ti-Nb-O martensitic alloy, Phys. Rev. B 82 (2010) 214104.
[21] S. Xu, J. Pons, R. Santamarta, I. Karaman, O. Benafan, R.D. Noebe, Strain glass state in Ni-rich Ni-Ti-Zr shape memory alloys, Acta Mater. 218 (2021) 117232.
[22] C. Lauhoff, A. Reul, D. Langenkämper, P. Krooß, C. Somsen, M.J. Gutmann, B. Pedersen, I.V. Kireeva, Y.I. Chumlyakov, G. Eggeler, W.W. Schmahl, T. Niendorf, Effects of aging on the stress-induced martensitic transformation and cyclic superelastic properties in Co-Ni-Ga shape memory alloy single crystals under compression, Acta Mater. 226 (2022) 117623.
[23] H.Z. Lu, H.W. Ma, W.S. Cai, X. Luo, Z. Wang, C.H. Song, S. Yin, C. Yang, Stable tensile recovery strain induced by a Ni_4Ti_3 nanoprecipitate in a $Ni_{50.4}Ti_{49.6}$ shape memory alloy fabricated via selective laser melting, Acta Mater. 219 (2021) 117261.
[24] A. Kosogor, V.A. L'vov, V.A. Chernenko, E. Villa, J.M. Barandiaran, T. Fukuda, T. Terai, T. Kakeshita, Hysteretic and anhysteretic tensile stress–strain behavior of Ni–Fe(Co)–Ga single crystal: experiment and theory, Acta Mater. 66 (2014) 79–85.
[25] H. Chen, Y.D. Wang, Z. Nie, R. Li, D. Cong, W. Liu, F. Ye, Y. Liu, P. Cao, F. Tian, X. Shen, R. Yu, L. Vitos, M. Zhang, S. Li, X. Zhang, H. Zheng, J.F. Mitchell, Y. Ren, Unprecedented non-hysteretic superelasticity of [001]-oriented NiCoFeGa single crystals, Nat. Mater. 19 (2020) 712–718.
[26] P. Cao, F. Tian, W. Li, L. Vitos, Y. Wang, Ideal superelasticity in Ni-based Heusler alloys, Acta Mater. 210 (2021) 116816.
[27] B. Wang, G. Kang, Q. Kan, W. Wu, K. Zhou, C. Yu, Atomistic study on the super-elasticity of nanocrystalline NiTi shape memory alloy subjected to a cyclic deformation, Comput. Mater. Sci. 142 (2018) 38–46.
[28] B. Wang, G. Kang, Q. Kan, W. Wu, K. Zhou, C. Yu, Atomistic study on the super-elasticity of single crystal bulk NiTi shape memory alloy under adiabatic condition, Comput. Mater. Sci. 152 (2018) 85–92.
[29] B. Wang, G. Kang, W. Wu, K. Zhou, Q. Kan, C. Yu, Molecular dynamics simulations on nanocrystalline super-elastic NiTi shape memory alloy by addressing transformation ratchettingn and its atomic mechanism, Int. J. Plast. 125 (2020) 374–394.

[30] B. Wang, G. Kang, C. Yu, B. Gu, W. Yuan, Molecular dynamics simulations on one-way shape memory effect of nanocrystalline NiTi shape memory alloy and its cyclic degeneration, Int. J. Mech. Sci. 211 (2021) 106777.
[31] M. Piao, S. Miyazaki, K. Otsuka, N. Nishida, Effects of Nb addition on the microstructure of Ti-Ni alloys, Mater. Trans. 33 (1992) 337–345.
[32] Q.C. Fan, Y. Zhang, Y.H. Zhang, Y.Y. Wang, E.H. Yan, S.K. Huang, Y.H. Wen, Influence of Ni/Ti ratio and Nb addition on martensite transformation behavior of NiTiNb alloys, J. Alloys Compd. 790 (2019) 1167–1176.
[33] B.J. Lee1, M.I. Baskes, Second nearest-neighbor modified embedded-atom-method potential, Phys. Rev. B 62 (2000) 8564–8567.
[34] W.S. Ko, B. Grabowski, J. Neugebauer, Development and application of a Ni-Ti interatomic potential with high predictive accuracy of the martensitic phase transition, Phys. Rev. B 92 (2015) 134107.
[35] W.S. Ko, S.B. Maisel, B. Grabowski, J.B. Jeon, J. Neugebauer, Atomic scale processes of phase transformations in nanocrystalline NiTi shape-memory alloys, Acta Mater. 123 (2017) 90–101.
[36] A. Ahadi, T. Kawasaki, S. Harjo, W.S. Ko, Q. Sun, K. Tsuchiya, Reversible elastocaloric effect at ultra-low temperatures in nanocrystalline shape memory alloys, Acta Mater. 165 (2019) 109–117.
[37] S. Nose, A unified formulation of the constant temperature molecular dynamics methods, J. Chem. Phys. 81 (1984) 511–519.
[38] M. Parrinello, A. Rahman, Polymorphic transitions in single crystals: a new molecular dynamics method, J. Appl. Phys. 52 (1998) 7182–7190.
[39] G.J. Ackland, A.P. Jones, Applications of local crystal structure measures in experiment and simulation, Phys. Rev. B 73 (2006) 054104.
[40] S. Plimpton, Fast parallel algorithms for short-range molecular-dynamics, J. Comput. Phys. 117 (1995) 1–19.
[41] A. Stukowski, Visualization and analysis of atomistic simulation data with OVITO – the open visualization tool, Modell. Simul. Mater. Sci. Eng. 18 (2010) 015012.
[42] Y. Wang, X. Ren, K. Otsuka, A. Saxena, Temperature – stress phase diagram of strain glass $Ti_{48.5}Ni_{51.5}$, Acta Mater. 56 (2008) 2885–2896.
[43] J. Zhang, Y. Wang, X. Ding, Z. Zhang, Y. Zhou, X. Ren, D. Wang, Y. Ji, M. Song, K. Otsuka, J. Sun, Spontaneous strain glass to martensite transition in a $Ti_{50}Ni_{44.5}Fe_{5.5}$ strain glass, Phys. Rev. B 84 (2011) 214201.
[44] Y. Wang, X. Ren, K. Otsuka, Shape memory effect and superelasticity in a strain glass alloy, Phys. Rev. Lett. 97 (2006) 225703.
[45] F. Xiao, T. Fukuda, T. Kakeshita, Critical point of martensitic transformation under stress in an Fe-31.2Pd (at.%) shape memory alloy, Philos. Mag. 95 (2015) 1390–1398.
[46] S. Picak, H.C. Yilmaz, I. Karaman, Simultaneous deformation twinning and martensitic transformation in CoCrFeMnNi high entropy alloy at high temperatures, Scr. Mater. 202 (2021) 113995.
[47] N. Ozdemir, I. Karaman, N.A. Mara, Y.I. Chumlyakov, H.E. Karaca, Size effects in the superelastic response of $Ni_{54}Fe_{19}Ga_{27}$ shape memory alloy pillars with a two stage martensitic transformation, Acta Mater. 60 (2012) 5670–5685.
[48] T. Waitz, H.P. Karnthaler, Martensitic transformation of NiTi nanocrystals embedded in an amorphous matrix, Acta Mater. 52 (2004) 5461–5469.
[49] T. Waitz, V. Kazykhanov, H.P. Karnthaler, Martensitic phase transformations in nanocrystalline NiTi studied by TEM, Acta Mater. 52 (2004) 137–147.
[50] Q. Sun, A. Aslan, M. Li, M. Chen, Effects of grain size on phase transition behavior of nanocrystalline shape memory alloys, Sci. Chin. Technol. Sci. 57 (2014) 671–679.
[51] Y. Wang, X. Ren, K. Otsuka, A. Saxena, Evidence for broken ergodicity in strain glass, Phys. Rev. B 76 (2007) 132201.
[52] Q. Liang, D. Wang, J. Zhang, Y. Ji, X. Ding, Y. Wang, X. Ren, Y. Wang, Novel B19' strain glass with large recoverable strain, Phys. Rev. Mater. 1 (2017) 033608.
[53] Y. Ji, D. Wang, Y. Wang, Y. Zhou, D. Xue, K. Otsuka, Y. Wang, X. Ren, Ferroic glasses, npj Comput. Mater. 3 (2017) 43.
[54] W. van Megen, S.M. Underwood, Glass transition in colloidal hard spheres: measurement and mode-coupling-theory analysis of the coherent intermediate scattering function, Phys. Rev. E 49 (1994) 4206–4220.
[55] Y. Wang, Y. Zhou, J. Zhang, X. Ding, S. Yang, X. Song, X. Ren, K. Otsuka, Evolution of the relaxation spectrum during the strain glass transition of $Ti_{48.5}Ni_{51.5}$ alloy, Acta Mater. 58 (2010) 4723–4729.
[56] H. Ramanarayan, T.A. Abinandanan, Phase field study of grain boundary effects on spinodal decomposition, Acta Mater. 51 (2003) 4761–4772.
[57] S. Rudraraju, A. Van der Ven, K. Garikipati, Mechanochemical spinodal decomposition: a phenomenological theory of phase transformations in multi-component, crystalline solids, npj Comput. Mater. 2 (2016) 16012.
[58] C.Y. Lo, K.S. Wu, E.H. Horng, A study of B2↔B19↔B19′ two-stage martensitic transformation in a $Ti_{50}Ni_{40}Cu_{10}$ alloy, Acta Metall. Mater. 41 (1993) 747–759.
[59] H. Tanaka, Liquid–liquid transition and polyamorphism, J. Chem. Phys. 153 (2020) 130901.
[60] Y.C. Xu, W.F. Rao, J.W. Morris, A.G. Khachaturyan, Nanoembryonic thermoelastic equilibrium and enhanced properties of defected pretransitional materials, npj Comput. Mater. 4 (2018) 58.
[61] B. Wang, F. Li, L.Q. Chen, Inverse domain-size dependence of piezoelectricity in ferroelectric crystals, Adv. Mater. (2021) 2105071.
[62] D. Wang, Y. Wang, Z. Zhang, X. Ren, Modeling abnormal strain states in ferroelastic systems: the role of point defects, Phys. Rev. Lett. 105 (2010) 205702.
[63] Y. Wang, J. Gao, H. Wu, S. Yang, X. Ding, D. Wang, X. Ren, Y. Wang, X. Song, J. Gao, Strain glass transition in a multifunctional β-type Ti alloy, Sci. Rep. 4 (2014) 3995.
[64] A. Ahadia, Q. Sun, Stress-induced nanoscale phase transition in superelastic NiTi by in situ X-ray diffraction, Acta Mater. 90 (2015) 272–281.
[65] P. Hua, M. Xia, Y. Onuki, Q. Sun, Nanocomposite NiTi shape memory alloy with high strength and fatigue resistance, Nat. Nanotechnol. 16 (2021) 409–413.
[66] H. Lin, P. Hua, Q. Sun, Effects of grain size and partial amorphization on elastocaloric cooling performance of nanostructured NiTi, Scr. Mater. 209 (2022) 114371.